



## Open Research Online

### Citation

Gérard, J.-C.; Soret, L.; Thomas, I. R.; Ristic, B.; Willame, Y.; Depiesse, C.; Vandaele, A. C.; Daerden, F.; Hubert, B.; Mason, J. P.; Patel, M. R. and López-Valverde, M. A. (2024). Observation of the Mars O<sub>2</sub> visible nightglow by the NOMAD spectrometer onboard the Trace Gas Orbiter. *Nature Astronomy*, 8 pp. 77–81.

### URL

<https://oro.open.ac.uk/94400/>

### License

(CC-BY-NC-ND 4.0) Creative Commons: Attribution-Noncommercial-No Derivative Works 4.0

<https://creativecommons.org/licenses/by-nc-nd/4.0/>

### Policy

This document has been downloaded from Open Research Online, The Open University's repository of research publications. This version is being made available in accordance with Open Research Online policies available from [Open Research Online \(ORO\) Policies](#)

### Versions

If this document is identified as the Author Accepted Manuscript it is the version after peer review but before type setting, copy editing or publisher branding

## **Observation of the Mars O<sub>2</sub> visible nightglow by TGO-NOMAD**

J.-C. Gérard<sup>1</sup>, L. Soret<sup>1</sup>, I.R. Thomas<sup>2</sup>, B. Ristic<sup>2</sup>, Y. Willame<sup>2</sup>,  
C. Depiesse<sup>2</sup>, A.C. Vandaele<sup>2</sup>, F. Daerden<sup>2</sup>, B. Hubert<sup>1</sup>, J. P. Mason<sup>3</sup>,  
M.R. Patel<sup>3</sup>, M.A. López-Valverde<sup>4</sup>

<sup>1</sup>LPAP, STAR Institute, Université de Liège, Belgium

<sup>2</sup>Royal Belgian Institute for Space Aeronomy, Brussels, Belgium

<sup>3</sup>School of Physical Sciences, The Open University, Milton Keynes, UK

<sup>4</sup>Instituto de Astrofísica de Andalucía/CSIC, Granada, Spain

<sup>5</sup>Istituto di Astrofisica e Planetologia Spaziali, INAF, Rome, Italy

Corresponding author: J.-C. Gérard  
email: [jc.gerard@uliege.be](mailto:jc.gerard@uliege.be)

September 1, 2023

Final

**On Mars, atomic oxygen controls the CO<sub>2</sub> radiative cooling of the upper atmosphere and the presence of an ozone layer near the south pole. In order to remotely probe meridional transport of O atoms from the summer to the winter hemisphere and the descending flow in the winter polar regions, the O<sub>2</sub> Herzberg II atmospheric emission could be used as a proxy. This emission is quite weak on the Earth's night side, but it is prominent in the Venus night airglow, and it has not previously been observed on Mars. Here, we report the limb detection of the O<sub>2</sub> Herzberg II visible bands in the Mars nightglow with the NOMAD-UVIS spectrometer on board ESA's Trace Gas orbiter. The emission layer reaches up to hundreds of kilometers in the limb viewing geometry. It is mainly located between 40 and 60 km at high latitudes during the winter season, consistent with three-body recombination of oxygen atoms. This O<sub>2</sub> nightglow should be observable from a Martian orbiter as well as from the Martian surface with the naked eye. These observations pave the way to future global observations of the Martian atmospheric circulation with simpler lower-cost instrumentation.**

The mesosphere of Venus and Mars is still poorly known as mesospheric data are scarce and Global Circulation Models can hardly reproduce them. Its composition, circulation pattern and variability are still not well understood. It is important to characterize the Martian mesosphere to determine the structure of the terrestrial planets' atmospheres and understand their different evolution. Observations of mesospheric airglow emissions is a powerful remote sensing tool that provides insight into the density variations and global transport in this region.

The Mars airglow emissions on the dayside have been extensively studied based on observations performed with instruments on board the Mariner, Mars Express (MEx), Mars Atmosphere and Volatile Evolution Mission (MAVEN), Trace Gas Orbiter (TGO) and HOPE Emirates missions (EMM). Following the first observations from the Mariner 6 and 7 flybys<sup>1</sup>, later studies have described the distribution of the ultraviolet CO Cameron, CO<sub>2</sub><sup>+</sup> UV doublet and Fox-Duffendack-Barker bands, H Lyman- $\alpha$ , O I 130 and 136 nm multiplets and N<sub>2</sub> Vegard-Kaplan emissions, their sources and dependence on latitude, solar longitude and solar activity. Recently, observations of the [OI] 557.7 nm and the 630-636 nm forbidden emissions made with the TGO Nadir and Occultation for Mars Discovery (NOMAD) instrument and their seasonal variability have been reported<sup>2,3,4,5</sup>.

On the night side, only the ultraviolet and infrared emissions have been explored with spectral instruments on board the MEx and MAVEN missions. The middle ultraviolet spectrum is dominated by the  $v'=0$   $\delta$  and  $\gamma$  bands of nitric oxide excited by radiative association of nitrogen and oxygen atoms. Although this emission is present at all latitudes and local times, extensive mapping has shown that it is enhanced in winter at high latitudes in both hemispheres<sup>6</sup>. This brightening is a consequence of the transport of O and N atoms from the summer to the winter hemisphere where they are carried downward by vertical winds and diffusion and recombine in the 40-60 km region. The O<sub>2</sub> Infrared Atmospheric

band at  $1.27 \mu\text{m}^{7,8,9}$  and the OH Meinel emission at  $1.45$  and  $2.9 \mu\text{m}^{10}$  have also been measured in the Martian polar winter atmosphere over a similar range of altitudes. They also result from meridional transport and winter polar descent of O atoms produced by photodissociation of  $\text{CO}_2$  in the summer hemisphere.

No nightglow spectrum has been observed so far in the visible domain. Scattered solar light hinders such measurements from the Earth's ground and no space-borne instrument has observed the Mars visible nightglow. In this report, we describe new observations made with the Ultraviolet and VISible (UVIS) channel, a spectrometer of the Nadir and Occultation for MArS Discovery (NOMAD) instrument flying on the ExoMars Trace Gas Orbiter. They cover both hemispheres, but their number is limited by operational constraints. Nevertheless, visible nightglow emissions have been observed for the first time on several TGO orbits. The observations reported here have been episodically collected between March 2020 and October 2022 with UVIS. The TGO satellite has been orbiting Mars since October 2016 on a circular orbit at  $\sim 400$  km, inclined  $74^\circ$  relative to the equator with an orbital period of  $\sim 2$  hours. The UVIS instrument is part of the NOMAD suite. It covers the 200-650 nm spectral range and can observe both in the nadir and solar occultation modes. The UVIS spectral resolution varies from 1.2 nm at 200 nm to 1.6 nm at 650 nm<sup>11,12</sup>. For the observations described in this study, the TGO spacecraft was oriented so that the line of sight of the nadir channel was pointing in the limb direction<sup>13</sup>. Two pointing modes were used during this period. In the first one, 'inertial pointing', the line of sight was kept fixed in the inertial space so that the line of sight scanned a range of altitudes usually from 300 km, down to 40 km, then up to 300 km. In the second one, most frequently used in this study, the areoid altitude of the tangent point in the atmosphere remained within  $\sim 20$  km of a pre-set value while different latitudes were probed due to the motion of the spacecraft. The spectra were integrated over 20 s. The resolution at the tangent point, taking into account the UVIS field of view during the spectral integration provided a vertical resolution of  $10 \pm 5$  km.

The NOMAD-UVIS instrument occasionally collected limb spectra during nightside conditions, with solar zenith angles greater than  $105^\circ$  at the tangent point of the line of sight. A band structure clearly appeared in some individual bright spectra between 400 and 600 nm. The wavelengths and relative intensities indicate coincidence with the strongest bands of the  $v'=0$  progression of the  $\text{O}_2$   $c^1\Sigma_u \rightarrow X^3\Sigma_g$  Herzberg II transition<sup>14</sup>.

A total of 1228 spectra have been acquired between 20 and 70 km and with a solar zenith angle  $>105^\circ$ , out of which 122 were kept. (see **Methods**). The average spectrum is shown in Fig. 1. The (0,5) to (0,11) Herzberg II bands are clearly identified with relative intensities similar to those observed on Venus<sup>15</sup> and in the laboratory<sup>16</sup>. Beyond 620 nm, the noise level increases, making detection of the (0,12) band uncertain.

The confirmed spectral detections spread over 13 orbits are shown in Fig. 2a and 2b. A first group of detections extends from  $50^\circ$  to  $81^\circ$  S when the solar longitude  $L_s$  varied from  $94^\circ$  to  $158^\circ$ . A second one covers the  $L_s$  range  $225^\circ$ - $330^\circ$  between  $65^\circ$  and  $81^\circ$  N. The mean spectrum is shown in Fig. 1. The total intensity for bands  $v''=5$  to 12 derived from the spectral fit combined with the relative band intensity in the laboratory is  $108 \pm 11$  kR. The

estimated error combines contributions from the absolute calibration and measurement noise including the uncertainty in the spectral baseline.

The observed wavelengths perfectly match those in the laboratory and Venus Herzberg II spectra. The small differences in relative band brightness in Fig 1. result from the presence of the background noise level in the UVIS data. The relative band intensities in the brightest individual spectra show excellent agreement of the spectral shape. There is no indication of a departure of the intensity distribution compared to the Venus or laboratory spectrum. By analogy with the Venus nightglow spectrum, the presence of other weak O<sub>2</sub> band systems, such as the Chamberlain A' <sup>3</sup>Δ<sub>u</sub> → a <sup>1</sup>Δ<sub>g</sub>, Herzberg I A <sup>3</sup>Σ<sub>u</sub> → X <sup>3</sup>Σ<sub>g</sub> and c <sup>1</sup>Σ<sub>u</sub> → a <sup>1</sup>Δ<sub>g</sub> bands, may be expected in the region of the (0-6) to (0-12) Herzberg II bands. On Venus, their contribution is about 7 %, 5 % and 4% of the Herzberg II intensity respectively<sup>15</sup>. However, the signal to noise ratio of the UVIS instrument is clearly too low to confirm their presence in the UVIS nightglow spectra.

In Fig. 2, inertial limbs detections are represented with dots while limb tracking observations are shown with triangles. Each dot colour corresponds to one TGO orbit. Grey symbols represent observations without detection. Fig. 2a illustrates the concentration of the detections under high-latitude winter conditions. Fig. 2b indicates that the visible nightglow is observed between 34 and 66 km, generally poleward of 60°. The statistics of the detections is too small to obtain a statistically significant mean limb profile.

Fig. 3a shows the histogram of the altitudes of the spectra binned into 1-km intervals corresponding to a positive detection at the R>0.32 level. A maximum of 35 detections is observed at 42 km. The brightest single spectrum reached an intensity of 290 kR at 41 km and 76° N. The detection lower limit for single 15-s spectra is on the order of 20±10 kR. Fig. 3b presents the histogram of the detection relative frequency of occurrence versus altitude. They are mainly grouped between 35 and 59 km. The highest value is also observed at 42 km where the occurrence is as large as 76%. The detection frequencies at higher altitudes remain below 10%.

The detection of the visible Herzberg II bands in the Mars dayglow makes its measurement a promising technique to derive the atomic oxygen density and its variations in the middle atmosphere. It is produced by three-body recombination of atomic oxygen, following the scheme:



This is the accepted mechanism for the excitation of the O<sub>2</sub> nightglow in atmospheres<sup>17</sup>. Models based solely on three-body recombination of O atoms have been shown to adequately explain the observed O<sub>2</sub> Herzberg II intensity in the Venus nightglow<sup>18</sup> and the O<sub>2</sub> <sup>1</sup>Δ nightglow on Mars. Other processes have been mentioned as potential sources of O<sub>2</sub> c molecules on Venus, but they have been considered negligible in models of the O Venus and Mars nightglow<sup>18,19</sup>. In the absence of evidence for other source processes, we consider process (1) as the only important source of O<sub>2</sub> c <sup>1</sup>Σ excitation.

Model simulations for a zonally averaged atmosphere have been performed for different  $L_s$  and latitudes in both hemispheres. The volume emission rate is calculated based on process (1) and the relevant MCD temperature and density distributions. Fig. 4 presents the calculated limb profile of the brightness of the Herzberg II bands. Slightly lower values are predicted at latitudes beyond  $75^\circ$  but they are expected to drop considerably at lower latitudes. The calculated peak brightness decreases to a few kR at  $60^\circ\text{N}$  and moves up to 58 km. For sake of completeness the calculated limb profile for  $L_s = 60^\circ\text{N}$  is also shown, although no nightglow observation has been performed in the limited data base. Some intensity measurements from individual spectra are also shown for comparison. They either closely agree with the model value ( $79^\circ\text{N}$ ,  $76^\circ\text{N}$ ,  $76^\circ\text{S}$ ) or exceed it by a factor of 2 ( $75^\circ\text{N}$ ). The measurement at  $L_s=50^\circ$ ,  $65^\circ\text{S}$  has been collected in May 2023 and shows a discrepancy relative to the model by about an order of magnitude. This suggests that the O density was significantly higher than the value predicted by the MCD at the time of the observations. This difference is observed at a moderately high latitude, suggesting that the modeled meridional transport does not provide enough O atoms at these lower latitudes. If discrepancies are demonstrated to be reliable, they should provide new insights into the dynamical processes in the atmosphere, thereby improving the reliability of 3-D GCMs. Additional observations are necessary to confirm whether the discrepancies at these latitudes are common or occasional.

The clear spectral signature and its analogy with the laboratory and Venus nightglow, together with the general agreement of the predicted altitude and brightness, all confirm that the observed spectrum is produced by three-body recombination of O atoms. The enhanced brightness at high latitudes is the signature of the global transport ascending from the sunlit summer polar regions and descending to the dark winter hemisphere.

The  $\text{O}_2 \text{ a}^1\Delta_g \rightarrow \text{X}^3\Sigma_g$  Infrared Atmospheric emission at  $1.27 \mu\text{m}$  is another recombination emission also observed in the Martian nightglow. The peak altitude of the emitting layer varies between 40 and 65 km reaching up to 12 MR at 40 km in both winter regions beyond  $\sim 70^\circ$  of latitude<sup>7,8,9</sup>. In the case of the  $\text{a}^1\Delta_g$  metastable state, the recombination efficiency of the O atoms is on the order of 70% and collisional deactivation is negligible at the altitude of the emitting layer. Consequently, the intensity of the Infrared Atmospheric system is about 60 times higher than the Herzberg II bands.

Collisions between O and  $\text{CO}_2$  in the thermosphere populate the vibrational levels of  $\text{CO}_2$ , resulting in enhanced radiation of the  $15\text{-}\mu\text{m}$  emission to space and atmospheric cooling<sup>20</sup>. Consequently, the O density governs the efficiency of the non-LTE radiative transfer cooling in the upper atmosphere. Although this process essentially occurs at higher altitude than most of the  $\text{O}_2$  airglow emission, the O peak density derived from the nightglow vertical profile may be used to constrain the O density at higher altitudes. Therefore, the determination of its distribution and variability is of prime importance in understanding and modelling the thermal structure of the Martian upper atmosphere. Transport of O atoms across the terminator also plays a key role as a precursor in the formation of an ozone layer near the south winter pole<sup>21</sup>.

Future measurements will allow better determining the emission peak altitude, its brightness and variability. They will provide unique constraints on three-dimensional models of the global circulation<sup>22</sup> and dynamical processes at play in the middle atmosphere. By accumulating nightside limb observations, it will be possible to describe the mean O density distribution at high winter latitudes and its variability. In particular, additional observations will determine how accurately the transition of the bright nightglow from one hemisphere to the other is predicted by 3-D models. The question of a possible hemispheric asymmetry in the spatio-temporal airglow distribution will also be examined based on a larger number of detections.

The brightness of the O<sub>2</sub> Herzberg bands of several hundred kilorayleighs in the visible opens the possibility to observe them in the Martian high-latitude regions with simple space-borne cameras in the visible domain. We also note that the sensitivity threshold of the human eye in the green for nightside scotopic vision is estimated on the order of 1 kR<sup>23</sup> decreasing at shorter and longer wavelengths<sup>24</sup>. For the Herzberg bands, which are widespread over most of the visible range, a likely wavelength-averaged threshold value is on the order of a few kR, much lower than the bright emission described in this report. The polar winter visible nightglow is therefore expected to be observable with the naked eye by future astronauts from orbit or the Martian ground. Incidentally, we note that the oxygen green line at 557.7 nm is not observed in UVIS bright individual spectra nor after co-addition of nightglow spectra (Fig. 1). This non-detection sets an upper limit of about 1 kR on the line brightness. It is in full agreement with its absence in the laboratory recombination spectra and the lack of detection by the Mars 5 visible spectrometer setting an upper limit of 50 rayleighs<sup>19</sup> on the nightglow limb brightness of the green line.

## Methods

### Data processing

During the pipeline processing of the spectra, the instrumental background and the dark current on the CCD frame are first removed. In a second step, the noise is corrected from cosmic rays, anomalous and hot pixels. Next, the 81 fully illuminated CCD lines are binned to increase the signal-to-noise ratio of the individual spectra. In a third step, the count rate is converted into physical units (kilorayleigh, 1 kR corresponds to a brightness of  $10^9$  photons  $\text{cm}^{-2} \text{s}^{-1}$  emitted in  $4\pi$  steradians), using laboratory measurements and in flight calibration<sup>25</sup>. In addition to the statistical error on the count rate and removal of the background noise, a possible systematic error of  $\sim 10\%$  is associated with the uncertainties of the absolute instrumental calibration.

For verification of positive spectral detections, we calculate the correlation coefficient between the individual NOMAD spectra and the Venus nightglow average spectrum<sup>26</sup>, between 410 and 560 nm at a resolution of 3 nm. This Venus reference spectrum was obtained by summing Venus Express-VIRTIS-M spectra of the nightglow collected between 92 and 100 km during a total of 120 hours<sup>26</sup>. The Venus reference spectrum has been scaled to the UVIS averaged spectrum, following a least-squares fit.

NOMAD-UVIS spectra with a linear correlation coefficient  $R > 0.32$  have been retained and those with a too low signal to noise ratio have been removed. Application of the statistical Fisher test indicates that this correlation coefficient is significantly different from zero with a confidence level of 99%. A subsequent visual examination identified a number of contaminated spectra that have been removed from the database.

### Model simulations

The volume emission rate of the band system based on process (1) is given by:

$$\eta(O_2) = \varepsilon K [O]^2 [M] \frac{A}{A + k_{CO_2} [CO_2] + k_O [O]} \quad (2)$$

where:

[M] is the total number density, [O] and [CO<sub>2</sub>] are the O and CO<sub>2</sub> densities from the Mars Climate Database

$\varepsilon = 0.03$  is the effective yield of the  $c^1\Sigma_u$  state including cascades from higher lying states,  $A = 0.17 \text{ s}^{-1}$  is the total transition probability of the c-X transition i.e. from (c,  $v'=0$ ) to all (X,  $v''$ )

$K = 7.5 \times 10^{-33} (T/300)^{-3.25}$  is the total recombination coefficient of the three-body recombination of O in CO<sub>2</sub>

$k_{CO_2} = 3.1 \times 10^{-16} \text{ cm}^{-3} \text{ s}^{-1}$  and  $k_O = 5.9 \times 10^{-12} \text{ cm}^{-3} \text{ s}^{-1}$  are the quenching coefficients of the  $c^1\Sigma_u$  state by CO<sub>2</sub> and O respectively.

We adopt values deduced from the studies of the Venus airglow<sup>19</sup> based on laboratory measurements<sup>17</sup> and Venus Express observations<sup>26,27</sup>. They have been slightly adapted to match the O<sub>2</sub> nightglow limb observations with the VIRTIS spectral imager<sup>28,29</sup>. The K coefficient and its temperature dependence are adopted from Smith and Robertson<sup>30</sup>. The recombination rate is multiplied by 2.5 to account for the higher efficiency of CO<sub>2</sub> relative to N<sub>2</sub> as a third body<sup>31</sup>. For comparison with our observations, the O and CO<sub>2</sub> densities are taken from the Mars Climate Database (MCD, version 6.1<sup>32</sup>) for minimum solar activity conditions. Limb profiles are calculated by integrating the volume emission rate along the line of sight.

### Data availability

The NOMAD-UVIS spectra may be downloaded from ESA's SA archives at <https://archives.esac.esa.int/psa/#!Table%20View/NOMAD=instrument> (select UVIS from the list of instruments and "Level 3 Calibrated" from the processing level). Observed limb intensities and model calculations supporting Figure 4 are available from BIRA-IASB repository <https://dx.doi.org/10.18758/71021084> or from the corresponding author upon reasonable request.



**Acknowledgements.** B.H. is research associate of the Belgian Fund for Scientific Research (FNRS). ExoMars is a space mission of ESA and Roscosmos. The NOMAD experiment is led by the IASB-BIRA, assisted by Co-PI teams from Spain (IAA-CSIC), Italy (INAF-IAPS) and the United Kingdom (The Open University). This project acknowledges funding from BELSPO, with the financial and contractual coordination by the ESA Prodex Office (PEA grant numbers 4000121493 and 4000129683). M.A.L.-V. and J.-J.L.-M. were supported by grant number PGC2018-101836-B-100 (MCIU/AEI/FEDER, EU) and CEX2021-001131-S funded by MCIN/AEI/ 10.13039/501100011033. We also acknowledge support from the UK Space Agency through grant numbers ST/V002295/1, ST/V005332/1, ST/Y000234/1 and ST/X006549/1" and the Italian Space Agency through grant number 2018-2-HH.0. We thank the ESA TGO team and its project scientists H. Svedhem and C. Wilson for supporting these observations.

**Author contributions.** J.-C. G and L. S. conceived the study and wrote the manuscript. Y. W., C. D., B. B., I.R.T. and J.P.M. calibrated the UVIS data and prepared the datasets. Observation planning was managed by J.-C. G., L. S, B. R., M. R. P., J.-J. L. M. A.-C. V. is the NOMAD Principal Investigator and M.R.P, J.L.-M. and G. B. are NOMAD Co-principal investigators. All authors contributed to discussion and comments on the manuscript.

**Competing interests.** The authors declare the following competing interests:  
The authors declare no competing interests.

## REFERENCES

1. Barth, C. A. et al. Mariner 6 and 7 ultraviolet spectrometer experiment: Upper atmosphere data. *J. Geophys. Res.* **76**, 2213-2227 (1971).
2. Gérard, J. C. et al. Detection of green line emission in the dayside atmosphere of Mars from NOMAD-TGO observations. *Nat. Astron.* **4**, 1049-1052 (2020).
3. Gérard, J. C. et al. First observation of the oxygen 630 nm emission in the Martian dayglow. *Geophys. Res. Lett.* **48**(8), e2020GL092334 (2021).
4. Aoki, S. et al. Density and temperature of the upper mesosphere and lower thermosphere of Mars retrieved from the OI 557.7 nm dayglow measured by TGO/NOMAD. *J. Geophys. Res.* **127**(6), e2022JE007206 (2022).
5. Soret, L. et al. The Mars oxygen visible dayglow: A Martian year of NOMAD/UVIS observations. *J. Geophys. Res.* **127**(6), e2022JE007220 (2022).
6. Schneider, N. M. et al. Imaging of Martian circulation patterns and atmospheric tides through MAVEN/IUVS nightglow observations. *J. Geophys. Res.* **125**(8), e2019JA027318 (2020).
7. Bertaux, J. L., Gondet, B., Lefèvre, F., Bibring, J. P., & Montmessin, F. First detection of O<sub>2</sub> 1.27 μm nightglow emission at Mars with OMEGA/MEX and comparison with general circulation model predictions. *J. Geophys. Res.* **117**(E11) (2012).
8. Fedorova, A. et al. The O<sub>2</sub> nightglow in the martian atmosphere by SPICAM onboard of Mars-Express. *Icarus* **219**(2), 596-608 (2012).
9. Clancy, R. T. et al. Extensive MRO CRISM observations of 1.27 μm O<sub>2</sub> airglow in Mars polar night and their comparison to MRO MCS temperature profiles and LMD GCM simulations. *J. Geophys. Res.* **117**(E11) (2012).
10. Clancy, R. T., et al. First detection of Mars atmospheric hydroxyl: CRISM Near-IR measurement versus LMD GCM simulation of OH Meinel band emission in the Mars polar winter atmosphere. *Icarus* **226**, 272-281 (2013).
11. Patel, M. R. et al. NOMAD spectrometer on the ExoMars trace gas orbiter mission: part 2-design, manufacturing, and testing of the ultraviolet and visible channel. *Appl. Optics* **56**, 2771-2782 (2017).
12. Vandaele, A. C., et al. An integrated suite of three spectrometers for the ExoMars trace gas mission: Technical description, science objectives and expected performance. *Space Sci. Rev.* **214**, 1-47 (2018).
13. López-Valverde, et al. Investigations of the Mars Upper Atmosphere with ExoMars Trace Gas Orbiter. *Space Sci. Rev.* **214**, 29 (2018).

14. Krupenie, P. H. The spectrum of molecular oxygen. *J. Phys. Chem. Ref. Data* **1**, 423-534 (1972).
15. Krasnopolsky, V.A. Venus spectroscopy in the 3000-8000 Å region by Veneras 9 and 10. In Hunten D.M., Colin, L., Donahue, T.M. & Moroz, V.I, University of Arizona Press, Tucson, AZ, 459-483 (1983).
16. Lawrence, G. M., C. A. Barth, & V. Argabright. Excitation of the Venus night airglow, *Science* **195**, 573– 574 (1977).
17. Slinger, T. G., & Copeland, R. A. Energetic oxygen in the upper atmosphere and the laboratory. *Chem. Rev.* **103**, 4731-4766 (2003).
18. Bougher, S. W., & Borucki, W. J. Venus O<sub>2</sub> visible and IR nightglow: Implications for lower thermosphere dynamics and chemistry. *J. Geophys. Res.* **99**(E2), 3759-3776 (1994).
19. Krasnopolsky, V. A. Excitation of the oxygen nightglow on the terrestrial planets. *Planet. Space Sci.* **59**, 754-766 (2011).
20. Bougher, S. W., Hunten, D. M., & Roble, R. G. (1994). CO<sub>2</sub> cooling in terrestrial planet thermospheres. *J. Geophys. Res.* **99**, 14609-14622.
21. Montmessin, F., & Lefèvre, F. (2013). Transport-driven formation of a polar ozone layer on Mars. *Nat. Geosci.* **6**, 930-933 (1994).
22. Forget, F. et al. Improved general circulation models of the Martian atmosphere from the surface to above 80 km. *J. Geophys. Res.* **104**, 24155-24175 (1999).
23. Omholt, A. The optical aurora (Vol. 4). Springer Science & Business Media (2012).
24. Lilensten, J. Prediction of blue, red and green aurorae at Mars. *Planet. Space Sci.* **115**, 48-56 (2015).
25. Willame, Y. et al.. Calibration of the NOMAD-UVIS data. *Planet. Space Sci.* **218**, 105504 (2022).
26. García Muñoz, A., Mills, F. P., Slinger, T. G., Piccioni, G., & Drossart, P. Visible and near-infrared nightglow of molecular oxygen in the atmosphere of Venus. *J. Geophys. Res.* **114**(E12) (2009).
27. García Muñoz, A. et al. Limb imaging of the Venus O<sub>2</sub> visible nightglow with the Venus Monitoring Camera. *Geophys. Res. Lett.* **40**, 2539-2543 (2013).
28. Gérard, J. C., Soret, L., Migliorini, A., & Piccioni G. Oxygen nightglow emissions of Venus: Vertical distribution and collisional quenching. *Icarus* **223**, 602-608 (2013).
29. Migliorini, A. et al. The characteristics of the O<sub>2</sub> Herzberg II and Chamberlain bands observed with VIRTIS/Venus Express. *Icarus* **223**, 609-614 (2013).

30. Smith, G. P., & Robertson, R. Temperature dependence of oxygen atom recombination in nitrogen after ozone photolysis. *Chem. Phys. Lett.* **458**, 6-10 (2008).
31. Nair, H., Allen, M., Anbar, A. D., Yung, Y. L., & Clancy, R. T. A photochemical model of the Martian atmosphere. *Icarus*, **111**, 124-150 (1994).
32. Millour, E. et al. The Mars Climate Database (Version 6.1), EPSC Abstracts Vol. **16**, EPSC2022-786, Granada (2022).

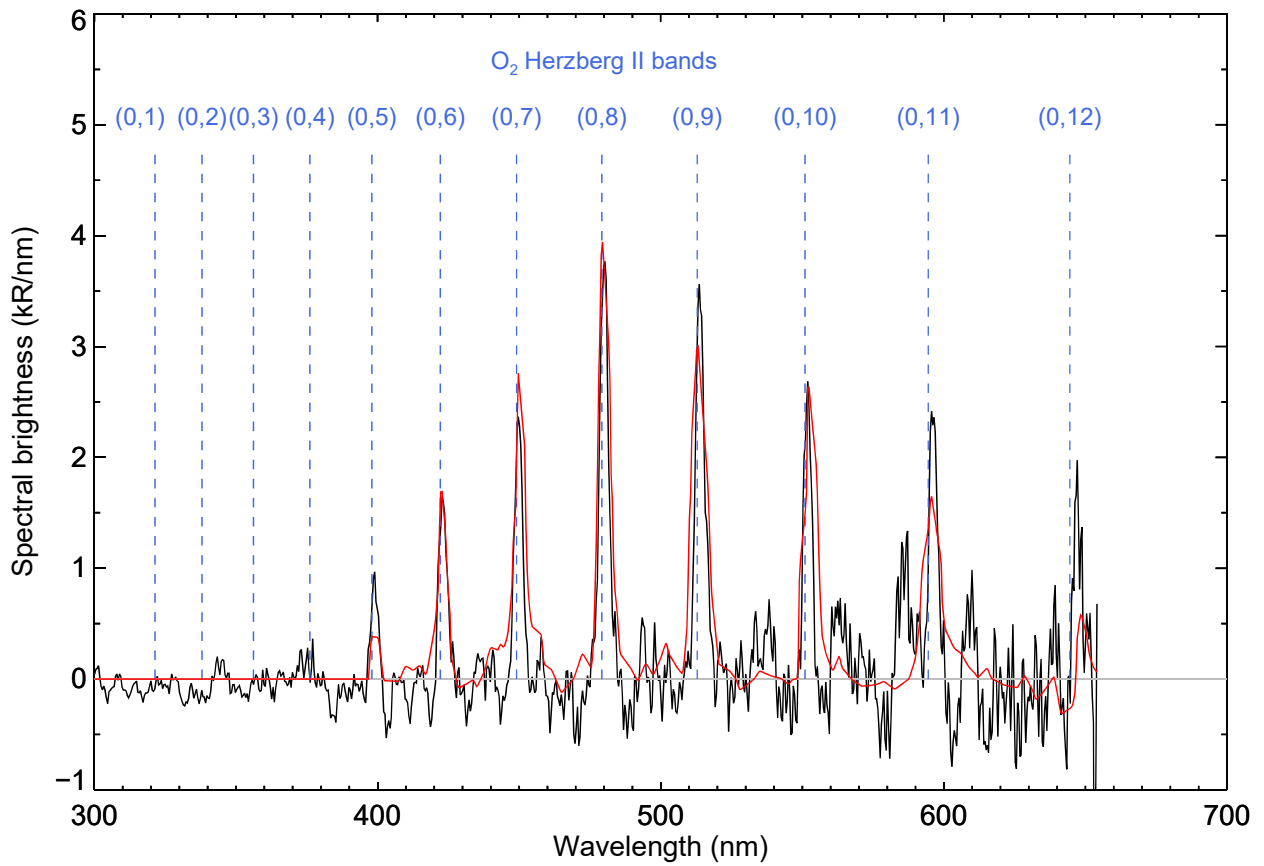


**Fig. 1. Average high-latitude nightglow spectrum.** The identifications of the  $v'=0$  Herzberg II bands are indicated by the vertical dotted lines. The red curve is the reference Venus nightglow spectrum scaled to the UVIS mean spectrum. A total of 122 high-latitude NOMAD-UVIS spectra have been averaged (black curve).

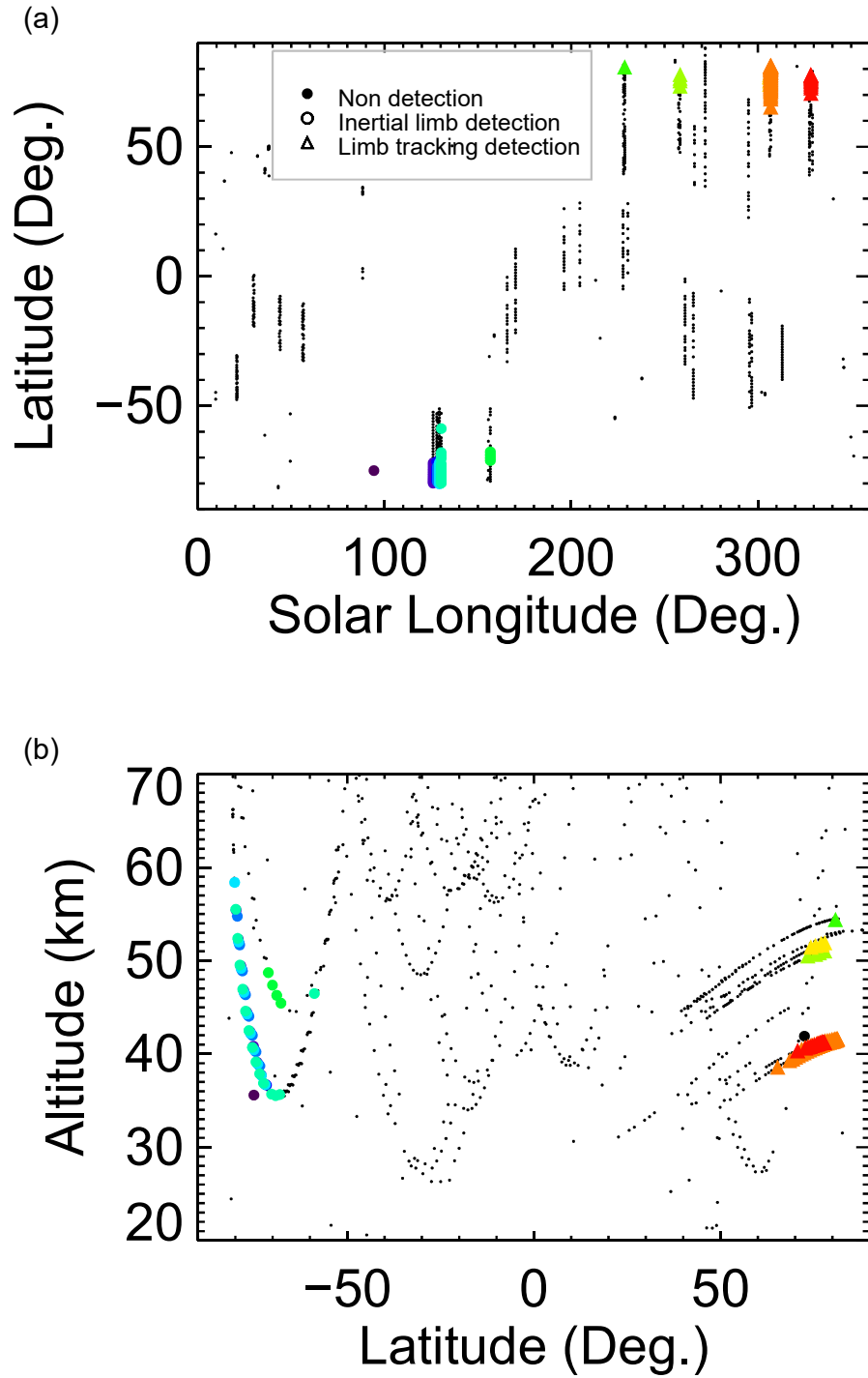


**Fig. 2. Distribution of detections of the O<sub>2</sub> Herzberg II nightglow.** a: latitude and season of the detections; b: areoid altitude-latitude map of the observations. The triangles indicate limb tracking and the dots inertial pointing orbits. Each dot colour corresponds to one TGO orbit. Small grey dots correspond to observations without measurable Herzberg II spectral signature.

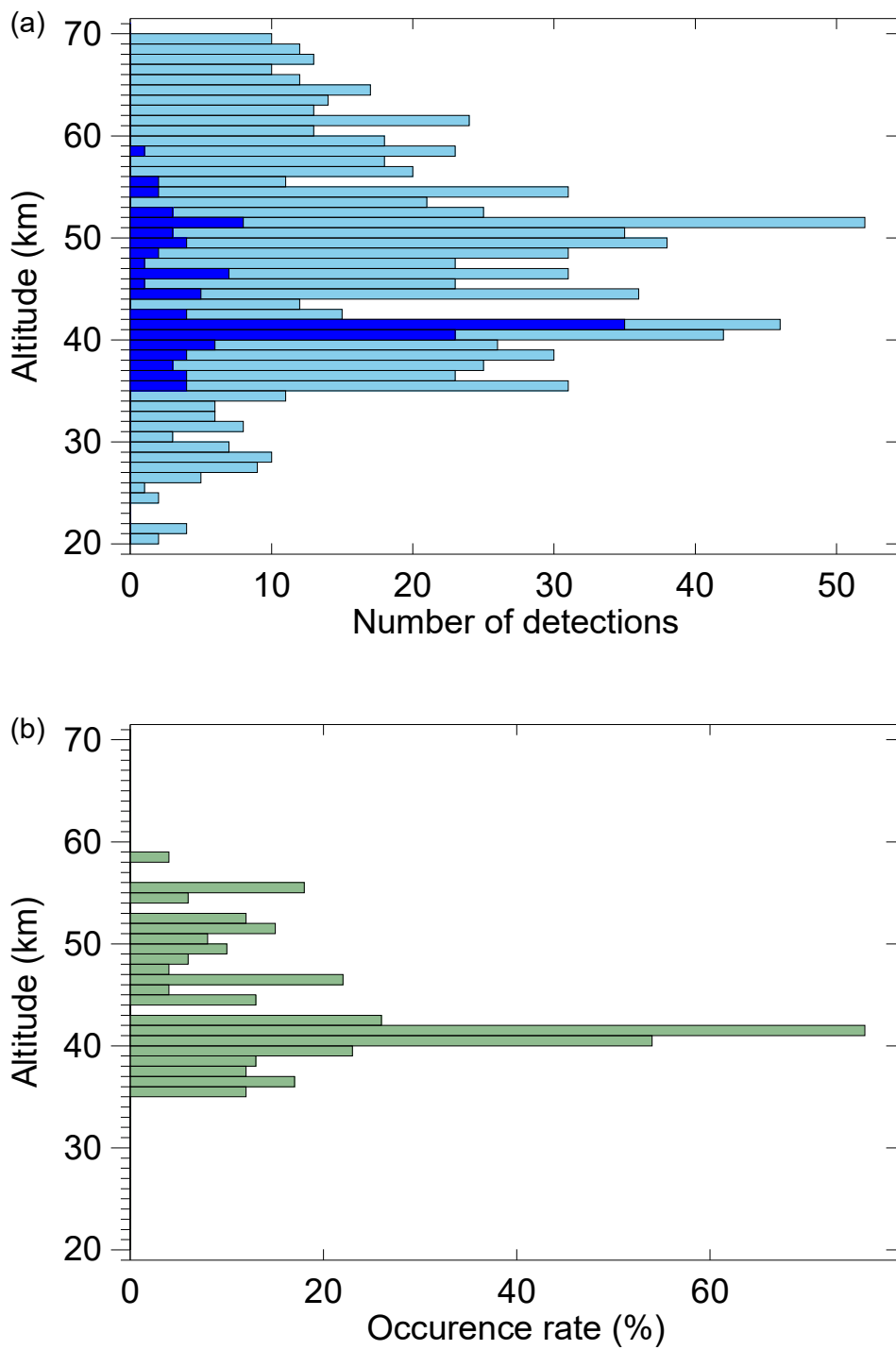


**Fig. 3. Altitude distribution of the nightside limb observations.** a: NOMAD-UVIS observations (light blue) and positive detections (dark blue); b: rate of occurrence of detections.

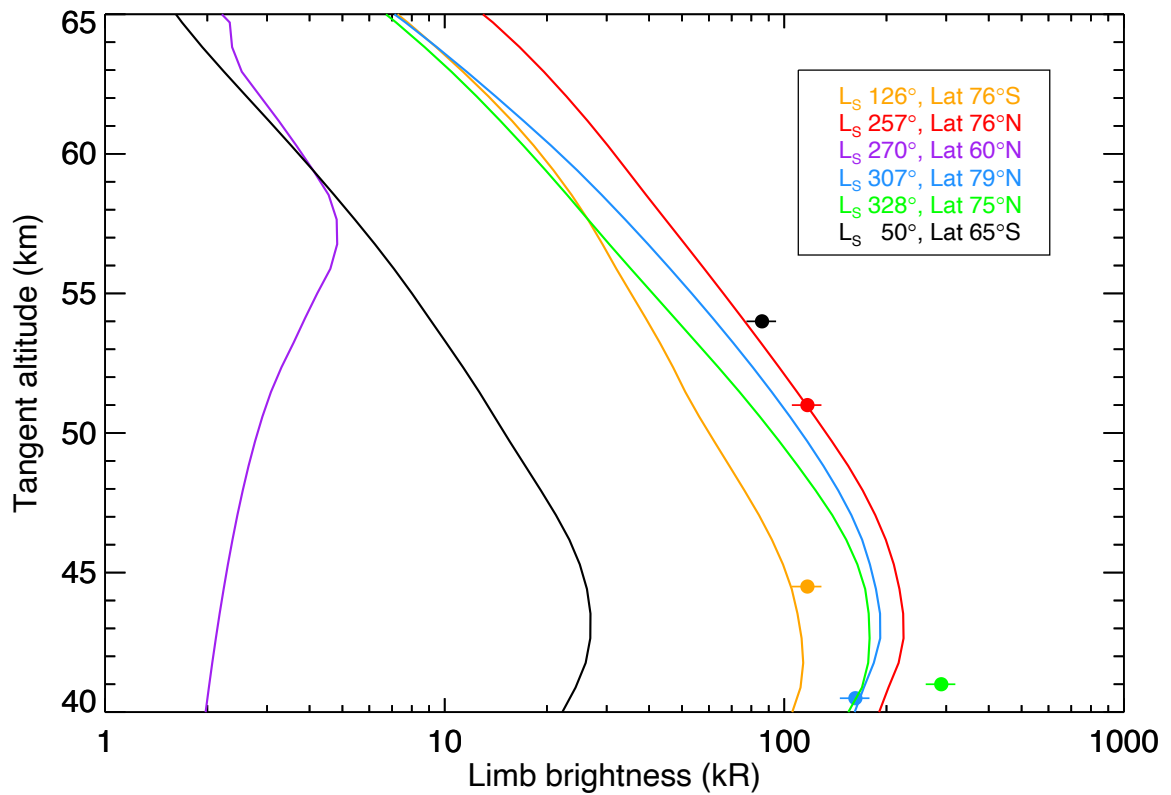


**Fig. 4. Model simulations of the limb brightness distribution of the O<sub>2</sub> Herzberg II bands.** The simulated limb profiles are calculated from expression 2 (methods) based on densities and temperature from the Mars Climate Database for different latitudes and seasons. The circles indicate UVIS observations using corresponding colours. The observed intensity values are 117 kR, 45 km (orange); 117 kR, 51 km (red); 162 kR, 40 km (blue); 290 kR, 41 km (green); 86 kR, 54 km (black). The error bars are estimated at 10% of the brightness. No detection at latitudes as low as 60°N is available in the current data base.